INTERNATIONAL JOURNAL FOR NUMERICAL METHODS IN FLUIDS
Int. J. Numer. Meth. Fluids 2000; **33**: 939–959

Finite difference scheme for the solution of fluid flow problems on non-staggered grids

I. E. Barton[a,*] and R. Kirby[b]

[a] *Department of Engineering, University of Cambridge, Trumpington Street, Cambridge, U.K.*
[b] *Department of Mechanical Engineering, Brunel University, Uxbridge, Middlesex, U.K.*

SUMMARY

A new finite difference methodology is developed for the solution of computational fluid dynamics problems that do not require the use of staggered grid systems. Previous successful and robust non-staggered methods, which used primitive variables and mass conservation in order to solve the pressure field, either interpolate cell-face velocities or interpolate the pressure gradients in a special way, usually with an upwind-bias to avoid the problem of odd–even coupling between the velocity and pressure fields. The new methodology presented does not detail a 'special interpolation procedure for a primitive variable', however, it manages to avoid the problem of odd–even coupling. The odd–even coupling is avoided by applying fourth-order dissipation to the pressure field. It is shown that this approach can be regarded as a modified Rhie and Chow scheme. The method is implemented using a SIMPLE-type algorithm and is applied to two test problems: laminar flow over a backward-facing step and laminar flow in a square cavity with a driven lid. Good agreement is obtained between the numerical solutions and the corresponding benchmark solutions. The pressure dissipation term was found to successfully suppress wiggles in the pressure field. Copyright © 2000 John Wiley & Sons, Ltd.

KEY WORDS: laminar flow; non-staggered grid method; odd–even coupling

1. INTRODUCTION

1.1. The problem

Primitive variable methodologies used to predict the Navier–Stokes equations using mass conservation to solve the pressure field are invariably solved on a staggered grid arrangement. The scalar properties including pressure are located at a different set of grid points compared with the velocity terms. This staggered arrangement is a well-known approach and has been

* Correspondence to: Department of Mechanical Engineering, Brunel University, Uxbridge, Middlesex, UB8 3PH, U.K.

Received November 1998
Revised May 1999

used with a variety of methodologies [1–4]. The main reason for using this arrangement is that it prevents odd–even coupling (sometimes referred to as checkerboarding) between the pressure field and the velocity fields; refer to Reference [5] for a further discussion of this problem. However, to a large degree this advantage is lost when developing 'mass conservation' methodologies, which either employ a curvilinear grid system, an unstructured grid system or a finite element framework, because the numerical code becomes arduous to develop. This difficulty has been detailed in Reference [6]. Although we are not considering any of these developments in this paper, this difficulty is the motivation for the development of a non-staggered scheme. The advantages of developing a non-staggered scheme are outlined in Reference [7].

There are two approaches to successfully curing the problem of odd–even coupling between the pressure and velocity fields. The first approach is to apply dissipation to the pressure field. A popular scheme to achieve this employs the technique of interpolating the cell-face velocities via 'momentum interpolation'; this was first proposed by Rhie and Chow [8] and has been followed by several investigators [9–18]. Rhie and Chow's approach can be considered essentially as a method to introduce fourth-order dissipation into the pressure field [19]. Some authors have approached the problem by explicitly adding this term in some form [20–22]. The second approach is not so well established. It uses a different interpolation scheme for the pressure gradients (in contrast with the cell-face velocity terms). A crude version of this approach was first presented in Reference [23]. More sophisticated versions using weighted upwind interpolation for the pressure gradients have been presented [24]. Even for advanced schemes [25,26] the secret of these approaches is that a different form of interpolation is being used. This resolves the problem. Therefore, one could argue that there are two approaches to resolving the problem of odd–even coupling. The first is to introduce some form of dissipation into the solution. The second is based on shifting the difficulty of dealing with the grid system to special interpolation schemes, which will effectively return the numerical code back to a staggered grid system. We can further argue that the second type of approach removes the problem by adding dissipation in a disguised form. We should finally note that there is a third option for a non-staggered methodology, which is to apply no special treatment to the discretized equations [27]. This may or may not lead to the prediction of a checkerboard distribution of pressure [26], whether it occurs or not is strongly dependent on the grid refinement, flow conditions and the boundary conditions implemented in the predictions [28].

1.2. The present contribution

In this paper, we build on the approach originated by Rhie and Chow [8] and add fourth-order dissipation to the pressure governing equation; however, unlike the majority of previous schemes, the dissipation is in a 'true' fourth-order form. We use finite difference techniques to derive the governing algebraic equations. This limits odd–even coupling occurring to a wavelength of 'one adjacent node' as opposed to 'two adjacent nodes', which would be the case if we used a fully discretized finite volume approach. The idea of reducing the 'natural wavelength of the pressure oscillations' has been previously proposed [29].

2. NUMERICAL ANALYSIS

2.1. Governing equations

The governing equations for momentum are based on simplified versions of the Navier–Stokes equations. We assume the flow is planar, constant density and we apply continuity to the viscous terms. The governing momentum equations are therefore expressed as

$$\frac{\partial \rho u}{\partial t}+\frac{\partial \rho u^2}{\partial x}+\frac{\partial \rho uv}{\partial y}=-\frac{\partial p}{\partial x}+\mu\left(\frac{\partial^2 u}{\partial x^2}+\frac{\partial^2 u}{\partial y^2}\right) \tag{1}$$

$$\frac{\partial \rho v}{\partial t}+\frac{\partial \rho uv}{\partial x}+\frac{\partial \rho v^2}{\partial y}=-\frac{\partial p}{\partial y}+\mu\left(\frac{\partial^2 v}{\partial x^2}+\frac{\partial^2 v}{\partial y^2}\right) \tag{2}$$

The governing equation of continuity is

$$\frac{\partial u}{\partial x}+\frac{\partial v}{\partial y}=0 \tag{3}$$

2.2. Discretization

Normally, the first step in the solution procedure is to discretize the above governing equations by applying conventional differencing techniques to the partial derivative terms [30]. In general form, following the notation of Patankar [5], the above equations can be expressed as

$$\left(A_P^u+\frac{\rho}{\Delta t}\right)u_P^*=\sum_M A_M^u u_M^*-\Delta_x p^0+u_P^0\frac{\rho}{\Delta t} \tag{4}$$

$$\left(A_P^v+\frac{\rho}{\Delta t}\right)v_P^*=\sum_M A_M^v v_M^*-\Delta_y p^0+v_P^0\frac{\rho}{\Delta t} \tag{5}$$

$$\Delta_x u^{**}+\Delta_y v^{**}=0 \tag{6}$$

The 'A' coefficients contain the discretized flux terms and diffusion terms for either the u momentum equation or the v momentum equation. These terms have been derived elsewhere [31]. The M index represents the nodes that form the surrounding computational molecule. The superscripts 0, * and ** refer to 'the last predicted solution', 'the first prediction level' and 'the correction level' respectively. The time derivative can either be treated as a 'real' or as a 'pseudo' time derivative term, which is incorporated into the solution procedure even for the solution of steady state problems in order to increase numerical stability [5]. When this set of discretized equations is implemented onto a control volume, the problem of odd–even coupling occurs at a wavelength of 'two adjacent nodes'. We postulate that the problem can be reduced if we adopt a slightly alternative approach, where we start by 'semi-discretizing' the governing equations to the following form:

$$\left(A_P^u + \frac{\rho}{\Delta t}\right)u_P^* = \sum_M A_M^u u_M^* - \frac{\partial p^0}{\partial x} + u_P^0 \frac{\rho}{\Delta t} \tag{7}$$

$$\left(A_P^v + \frac{\rho}{\Delta t}\right)v_P^* = \sum_M A_M^v v_M^* - \frac{\partial p^0}{\partial y} + v_P^0 \frac{\rho}{\Delta t} \tag{8}$$

$$\frac{\partial u^{**}}{\partial x} + \frac{\partial v^{**}}{\partial y} = 0 \tag{9}$$

We now employ this set of semi-discretized equations into a solution algorithm. In this paper, the solution of the governing equations is based on the standard SIMPLE algorithm [5]. The algorithm solves the pressure field by ensuring mass continuity is satisfied. Initially, the algorithm predicts the velocity field based on the current pressure field. This is achieved by solving Equations (4) and (5) for u^* and v^*; in doing so we argue that Equations (7) and (8) have been solved. The second step requires the use of an intermediate set of momentum equations to derive a pressure correction equation. The intermediate equations can be expressed as

$$\left(A_P^u + \frac{\rho}{\Delta t}\right)u_P^{**} = \sum_M A_M^u u_M^* - \frac{\partial p^*}{\partial x} + u_P^0 \frac{\rho}{\Delta t} \tag{10}$$

$$\left(A_P^v + \frac{\rho}{\Delta t}\right)v_P^{**} = \sum_M A_M^v v_M^* - \frac{\partial p^*}{\partial y} + v_P^0 \frac{\rho}{\Delta t} \tag{11}$$

These equations are not solved directly but are used to derive a pressure correction equation. This is achieved by respectively taking Equations (11) and (10) away from Equations (8) and (7), obtaining the following expressions:

$$u_P^{**} = u_P^* - \left(\frac{\partial p'}{\partial x}\right) \Big/ B_P^u \tag{12}$$

$$v_P^{**} = v_P^* - \left(\frac{\partial p'}{\partial y}\right) \Big/ B_P^v \tag{13}$$

where p' is the pressure correction, $p^* - p^0$ and B_P represent the discretized spatial and temporal terms of the pole coefficients in Equations (10) and (11) respectively. The argument of using 'intermediate momentum equations' is found in Reference [3] when developing the pressure implicit with splitting operators (PISO) scheme; alternatively we can follow the argument of Patankar [5], where the 'velocity corrections are ignored'. We considered that the second argument is less rigorous.

Next, Equations (12) and (13) are directly substituted into Equation (9), which leads to the following expression:

$$0 = \frac{\partial u_P^*}{\partial x} + \frac{\partial v_P^*}{\partial y} - \left(\frac{\partial}{\partial x} \frac{1}{B_P^u} \frac{\partial p'}{\partial x} + \frac{\partial}{\partial y} \frac{1}{B_P^v} \frac{\partial p'}{\partial y} \right) \tag{14}$$

This expression forms the Poisson pressure correction equation used to predict the pressure field. After its solution, values of p' can be substituted into Equations (12) and (13) and so u_P^{**} and v_P^{**} can be calculated. Equation (14) is expressed in semi-discretized form and therefore needs to be fully discretized. It is straightforward to go back and discretize Equations (12) and (13). For Equation (14) we use modified central differencing for the second-order derivative terms, and we integrate the equation around a control volume for the continuity term. We approximate the second-order derivative term as follows:

$$\text{If } \frac{\partial^2 \phi}{\partial x^2} \approx \nabla^2 \phi = \sum_M A_M (\phi_M - \phi_P)$$

$$\text{Let } \frac{\partial}{\partial x} \frac{1}{B_P} \frac{\partial \phi}{\partial x} \approx \sum_M \frac{2A_M}{B_M + B_P} (\phi_M - \phi_P) \tag{15}$$

A similar approach is adopted in Reference [32], where they assume a harmonic average of the B coefficients.

So far, we have detailed a scheme where odd–even coupling may or may not occur. It is, in fact, a better approach at avoiding odd–even coupling than using 'standard discretization', because a compact Laplacian is formed for the pressure correction equation. We now postulate a theory for removing the odd–even coupling. We start by introducing the following operator $\vee^2$, which is simply a 'non-dimensionalized' discretized second-order differential term, expressed as

$$\text{If } \frac{\partial^2 \phi}{\partial x^2} \approx \nabla^2 \phi = \sum_M A_M (\phi_M - \phi_P)$$

$$\text{Let } \vee^2 \phi = \frac{\sum_M A_M (\phi_M - \phi_P)}{A_P}$$

$$\text{where } A_P = \sum_M A_M \tag{16}$$

It is straightforward to show that for a Cartesian grid

$$\frac{\Delta x_e \Delta x_w}{2} \frac{d^2 \phi}{dx^2} \approx \vee_x^2 \phi \tag{17}$$

where 'e' and 'w' refer to the 'east' and 'west' cell lengths. Also, we can show that

$$\frac{\Delta x_e \Delta x_w}{2} \frac{d^4\phi}{dx^4} \approx \nabla_x^2 \vee_x^2 \phi \tag{18}$$

The dissipation term added to the governing pressure equation used in the Rhie and Chow [8] methodology is not expressed directly in their paper, but we could express it as

$$\text{dissipation} = {}_{2\delta}\nabla^2 p / B_P^{2\delta} - {}_{1\delta}\nabla^2 p / B_P^{1\delta} \tag{19}$$

where the operators ${}_{2\delta}\nabla^2$ and ${}_{1\delta}\nabla^2$ refer to the discretized second-order derivative taken on a grid with 2-nodal and 1-nodal spacing. We can approximate this difference as a fourth-order term if we assume slow variation in the coefficient B. For example, referring to Hirsch [33] and using uniform spacing, we find that

$${}_{2\delta}\nabla^2 p - {}_{1\delta}\nabla^2 p \cong \frac{\Delta x^2}{4} {}_{1\delta}\nabla^4 p + O(\Delta x^4) \tag{20}$$

Thus, the Rhie and Chow [8] methodology approximately applies a fourth-order dissipation term. In this paper we assume that the variation of $B_P^{2\delta}$ and $B_P^{1\delta}$ is so small that we can justify the application of a 'true' fourth-order dissipation term in the form of Equation (18).

2.3. An aside about the $\vee^2$ operator

The non-dimensionalized second-order derivative term is a useful operator. For example, we can use it to smooth a field variable

$$\phi^{\text{smooth}} = \phi + \sigma(\vee_x^2 + \vee_y^2)\phi \tag{21}$$

where $0 < \sigma \ll 1$ will be a parameter that will successfully smooth the results. Also, it can be used to 'model' differential terms, such as the first-order or second-order terms, with a higher degree of accuracy using 1-nodal spacing approximations in order to achieve accuracy greater than the second-order. For example

$$\frac{d\phi}{dx} \cong \nabla_x \phi - \frac{1}{3} \nabla_x \vee_x^2 \phi + O(\Delta x^4) \tag{22}$$

and

$$\frac{d^2\phi}{dx^2} \cong \nabla_x^2 \phi - \frac{1}{6} \nabla_x^2 \vee_x^2 \phi + O(\Delta x^4) \tag{23}$$

2.4. The dissipation term

Following on from Rhie and Chow [8] we could elect to add the following dissipation term into the governing pressure equation (14)

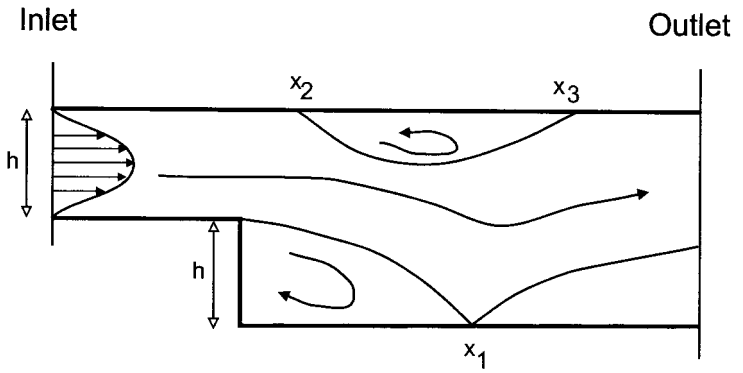

Figure 1. Illustration of the flow over a backward-facing step, showing a main reattachment region which attaches at x_1, an upper recirculation region, which separates at x_2 and reattaches at x_3.

$$\text{dissipation} = \alpha\left(\frac{\nabla_x^2 \vee {}_x^2 p}{B_P^u} + \frac{\nabla_y^2 \vee {}_y^2 p}{B_P^v}\right) \tag{24}$$

From Rhie and Chow and referring back to Equation (20), we know that $\alpha = 0.5$; however, it has been pointed out there is a problem with the Rhie and Chow methodology because the smoothing is dependent on the time step and the underrelaxation factor [9,34]. To remove this problem we solve the governing pressure correction equation using B coefficients that only contain the geometry terms; all other terms (temporal and pseudo-temporal) are neglected. In this case, the value of α should be constant even if there is a variation in the value of the underrelaxation and/or time step. Thus, in this paper, α was set to 0.04 for the example problems.

2.5. *Differencing scheme*

It is interesting to note that, because a non-staggered grid is employed in the present study, we need to introduce dissipation into the pressure field in order to remove unrealistic oscillations. This approach seems to be quite a foreign idea; however, introducing artificial viscosity in order to obtain numerically stable solutions for the velocity field is a well-established technique

Table I. Predictions of the main reattachment and separation positions at an inlet Reynolds number of $Re = 800$.

	x_1	x_2	x_3
FOAV No pressure dissipation	9.86	7.96	16.93
FOAV Applied pressure dissipation	9.74	7.85	16.80
SOAV No pressure dissipation	12.04	10.06	19.93
SOAV Applied pressure dissipation	12.02	10.05	19.80
Barton [36]	12.03	9.64	20.96

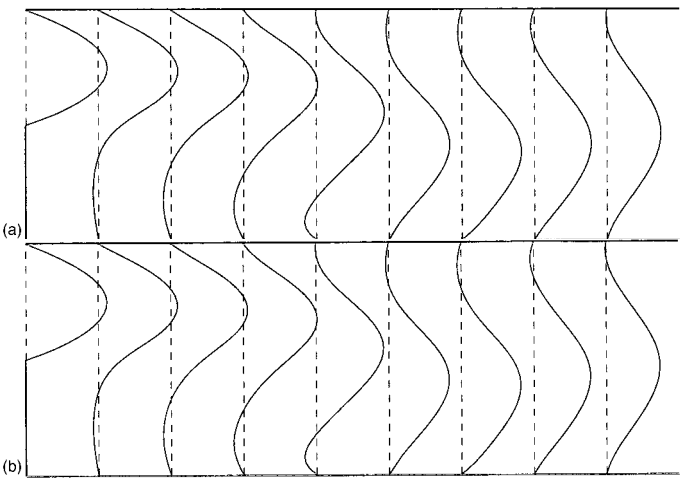

Figure 2. U velocity profiles at various positions, relative to the step they at $x = 0$, 2, 4, 6, 8, 10, 12, 14, 16 step heights downstream for the FOAV scheme; (a) no pressure dissipation and (b) applied pressure dissipation.

[35]. In the present investigation, two crude differencing schemes are employed that do not use an upwind bias, which is standard practice [36]. (The reason for this is the code was based on a finite element development that did not incorporate an upwind bias.) Both differencing schemes implemented work in the same way by applying additional viscosity such that the ratio of the most negative coefficient component compared with the pole coefficient is at least greater than negative unity (the ratio excludes temporal terms). This is approximately the minimum amount of additional viscosity that can be applied in order to achieve numerical stability. The first scheme is approximately first-order accurate and uses a 5-node molecule in the form of a cross and is referred to as first-order additional viscosity (FOAV). The second scheme is approximately second-order accurate it uses a 9-node molecule, again in the form of a cross. We refer to this scheme as second-order additional viscosity (SOAV).

We do not argue that these differencing schemes are superior to other schemes, they have been mainly used out of convenience. Further to this we need to make the point that the differencing scheme and the suppression of pressure oscillations are almost separate issues. Therefore, any differencing scheme can be used to demonstrate the pressure dissipation scheme. In order to test the authority of the schemes, comparisons were made for the square cavity flow using the first-order upwind differencing (FOUD) scheme [37]. These results were undertaken mainly to double-check the trends with regard to problems with pressure oscillations. Predictions using FOUD and by the FOAV scheme, found similar results with regard to suppressing the pressure oscillations; however, differences were found due to the hyperbolic nature of the FOUD scheme.

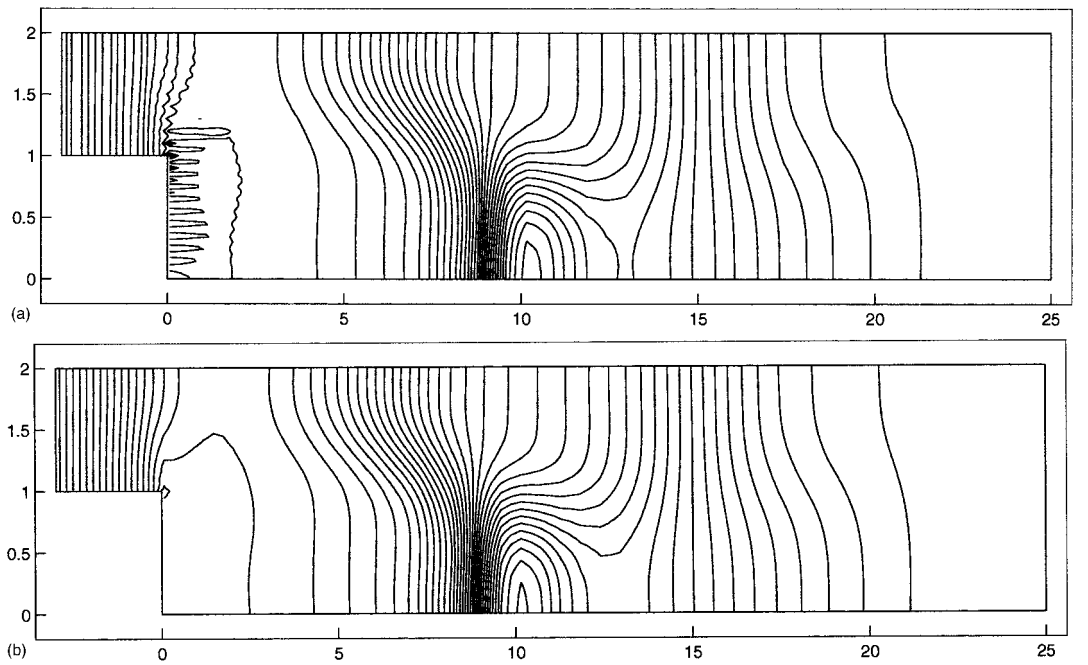

Figure 3. A contour plot of the pressure field in the main body of the channel for the FOAV scheme; (a) no pressure dissipation and (b) applied pressure dissipation.

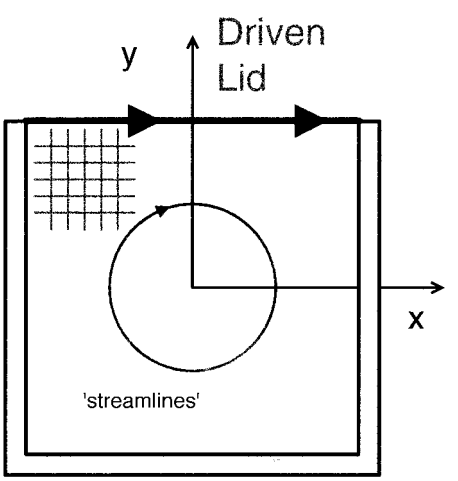

Figure 4. An illustration of the moving lid problem depicting the flow within the square cavity.

2.6. Matrix solver

The discretized equations of u, v and p are solved using the tri-diagonal matrix algorithm [35]. The algorithm sweeps through the solution domain until the residuals reduce by four orders of magnitude. Typically, overall changes in the velocity fields and pressure field are recorded until the changes reduce by at least six orders of magnitude and the source term in the pressure correction equation reduces by at least five orders of magnitude.

2.7. Boundary conditions

Where necessary, the methodology applies the following boundary conditions: first-order upwind interpolation is applied at the outlet boundary in order to extrapolate the outlet velocities. Inlet velocity values are prescribed. No-slip boundary conditions are applied at the walls simply by setting velocity terms to zero. Second-order extrapolation is applied along normal gradients for the pressure field for the inlet and outlet boundaries. Third-order extrapolation is applied for the flat wall boundaries; greater accuracy is achieved because the condition that

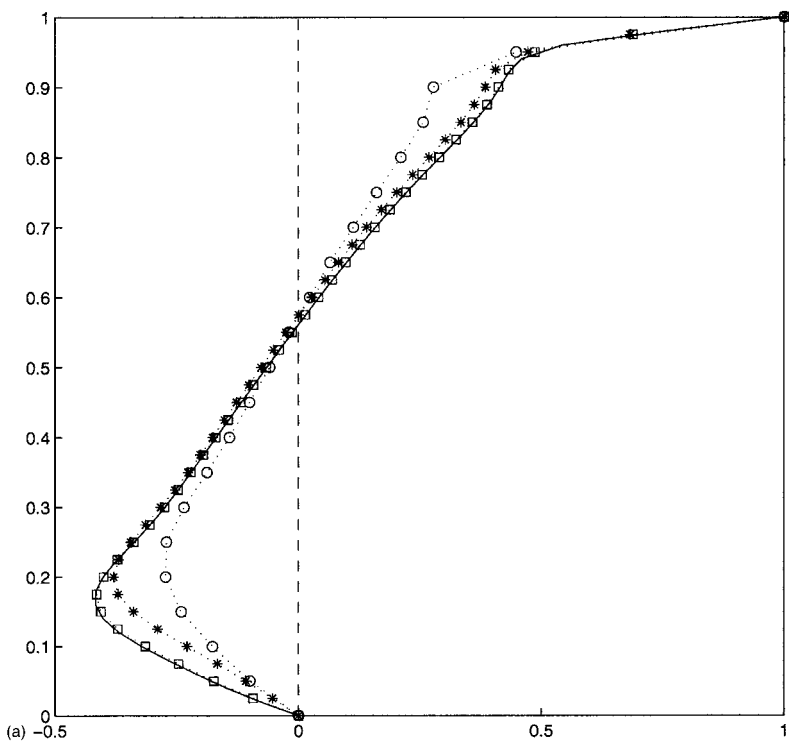

Figure 5. Velocity profiles along the centreline of the cavity for $Re = 1000$ using the SOAV scheme, using 20×20 grid ○, 40×40 grid ∗, 60×60 grid □ and a 100×100 grid (—) for (a) no pressure dissipation and (b) applied pressure dissipation.

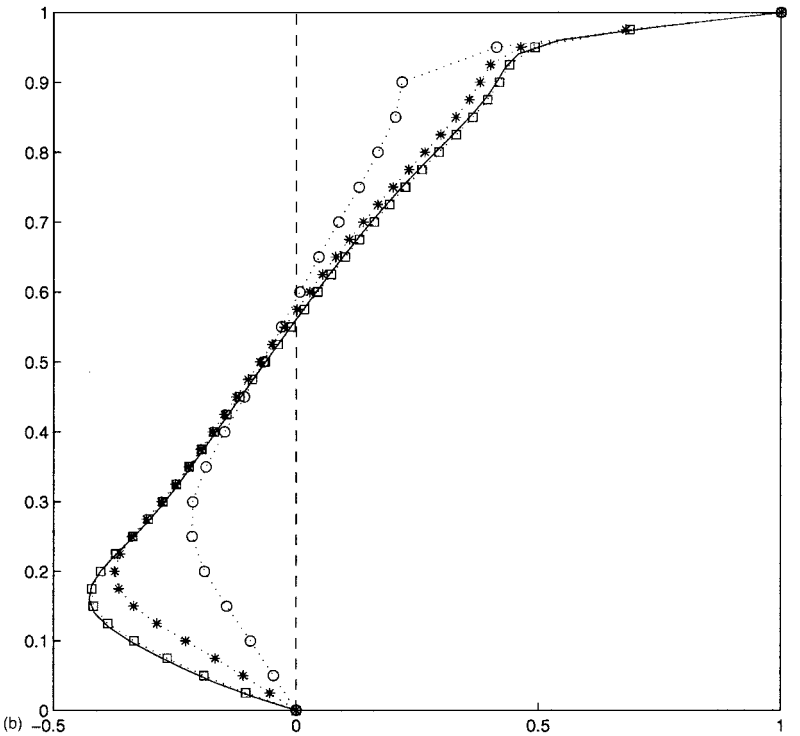

Figure 5 (*Continued*)

$$\left.\frac{\partial p}{\partial n}\right|_{\text{Wall}} = 0 \tag{25}$$

is incorporated into the extrapolation.

3. EXAMPLE APPLICATIONS

The non-staggered scheme is applied to two example applications: laminar flow over a backward-facing step and laminar flow in a square cavity with a driven lid. There are various benchmark solutions for these two applications.

3.1. Flow over a backward-facing step

Flow over a backward-facing step is one of the simplest flow problems where flow separation and reattachment occurs. The present research considers flow over a backward-facing step in a planar duct; a similar configuration has been experimentally and numerically studied by Armaly *et al.* [38]. Computations of this backward-facing step geometry have been made by a

large number of authors [32,39–42]. The flow configuration is illustrated in Figure 1. The problem prescribes a parabola u velocity profile at the inlet boundary. The step height and the height of the inlet channel are the same. The Reynolds number is set to $Re = 800$. This test case has become a standard numerical test [43]. The Reynolds number is defined using twice the step height as the length scale, the mean inlet velocity and the fluid's dynamic viscosity [38]. The problem domain is 30 step heights long in the main channel and 6 step heights long for the inlet channel.

The computations are undertaken on a non-uniform grid distribution in the x-direction and a uniform grid distribution in the y-direction. The grid system uses 80×40 grid points. There is grid refinement close to the step wall. This grid distribution is relatively coarse compared with grid independent results undertaken in Reference [36], where second-order accurate differencing schemes are applied. A coarse grid is applied so that the results will experience pressure oscillations. The problems with odd–even coupling are strongly related to the grid refinement and to the flow conditions, to a lesser degree the type of differencing scheme applied plays at part. The moderately refined grid used in this paper makes the problem a

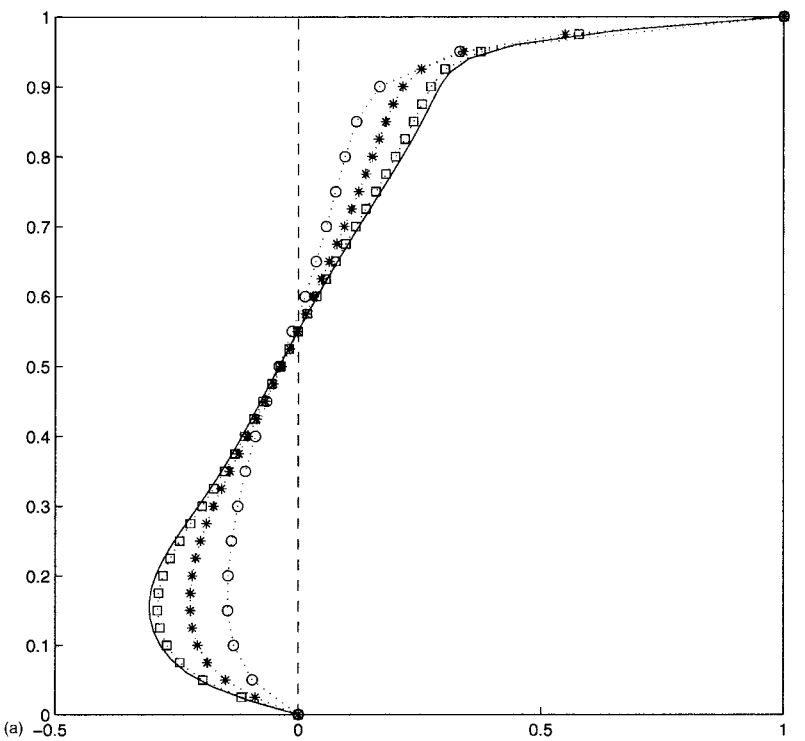

Figure 6. Velocity profiles along the centreline of the cavity for $Re = 1000$ using the FOAV scheme, using 20×20 grid ○, 40×40 grid ∗, 60×60 grid □ and a 100×100 grid (—) for (a) no pressure dissipation and (b) applied pressure dissipation.

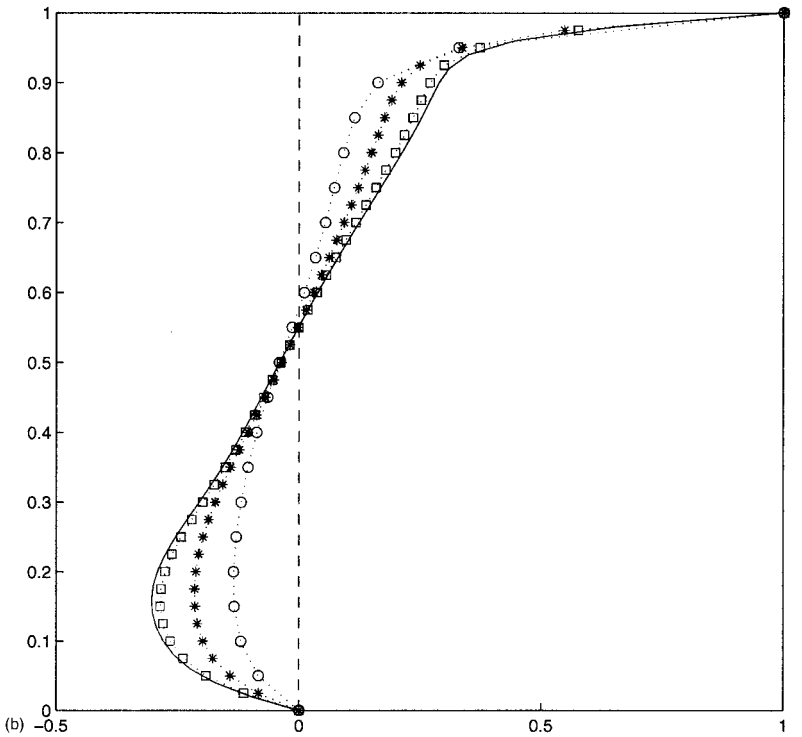

Figure 6 (*Continued*)

reasonable test for the non-staggered methodology because the flow pattern could be solved on a finer grid that would not require special non-staggered treatment. There are numerous predictions of this problem; a recent review is given in Reference [42]. It is sufficient to say that recent accurate predictions have been detailed in References [36,40,43].

The illustration in Figure 1 shows that there is a main recirculation region with a reattachment at x_1. The Reynolds number is sufficiently large to cause a strong adverse pressure gradient along the upper boundary that causes separation at x_2, the flow then reattaches at x_3. The results for the reattachment and separation positions are shown in Table I. Predictions are shown for the FOAV and SOAV schemes, which apply the pressure dissipation term and predictions that do not apply it. Table I also shows the grid-independent results from the study of Barton [36].

First, we will consider the overall predictions in comparison with grid-independent results. Compared with the grid independent results, the FOAV scheme underpredicts the reattachment and separation positions; however, the SOAV scheme predicts similar results to the grid-independent results. Despite the failings of the FOAV scheme there is a reasonably large upper recirculation region that is being predicted. The underpredictions of the reattachment and separation points compared with grid independent results is to be expected, similar results

have been predicted elsewhere most notably in Armaly *et al.* [38]. Their study used a standard first-order upwind differencing (FOUD) scheme. The FOAV scheme predicts overall better results than Armaly *et al.*, admittedly on a different grid system. Nonetheless, the study of Armaly *et al.* obtained a main reattachment that tends to agree with the grid-independent results; however, it fails to predict an upper recirculation that is in good agreement with the grid-independent results. This is a reflection of the FOUD scheme having similar accuracy compared with the FOAV scheme but also, it shows that the first-order upwind differencing scheme models the hyperbolic nature of the flow to a greater degree. This has the advantage of predicting more accurately results immediately downstream, but the probable disadvantage that the 'overall flow pattern' maybe somewhat distorted. The FOAV scheme models the elliptic nature of the flow to a greater degree, therefore, a large upper recirculation region is predicted for this scheme in comparison FOUD. The accuracy of the SOAV scheme is such that its results are similar to the grid-independent results, and therefore there is very little we can conclude from the demonstration, except that the differencing scheme must be working successfully.

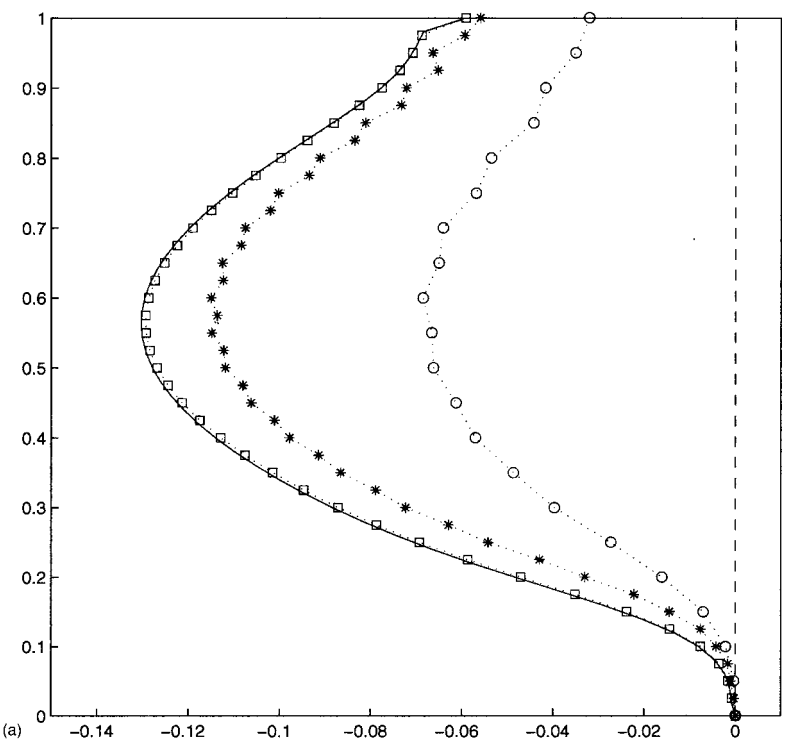

Figure 7. Pressure variation along the centreline of the cavity for $Re = 1000$ using the SOAV scheme, using 20×20 grid ○, 40×40 grid ∗, 60×60 grid □ and a 100×100 grid (—) for (a) no pressure dissipation and (b) applied pressure dissipation.

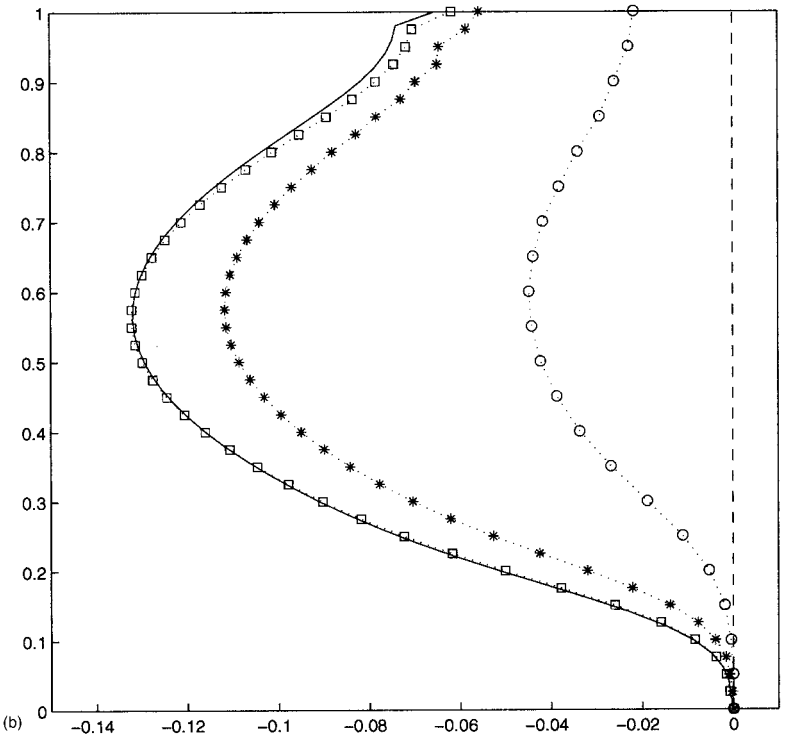

Figure 7 (*Continued*)

Next, we address the more important question which is what affect does the application of the pressure dissipation term have to the results? Does the pressure dissipation term affect the velocity field? And are there any wiggles in the pressure solution? The velocity profiles are found to be virtually identical with or without the application of pressure dissipation; this is confirmed in Table I, where the reattachment and separation positions are very similar. The difference between the results that apply pressure dissipation and those that do not is at most a tenth of a step height in length. This is equivalent to a difference of about 1 per cent; therefore, the application of the pressure dissipation term is having very little effect on the overall velocity field. Though, it has to be admitted that, the application of pressure dissipation term does slightly worsen the velocity predictions in comparison with grid independent results. In Figure 2 we show predictions of the velocity profiles for the FOAV scheme; Figure 2(a) shows predictions where no dissipation is applied and Figure 2(b) shows predictions where it is. These profiles show that there certainly is not any discernible difference in the velocity fields. For the SOAV scheme we again confirm that there is no discernible difference in the velocity fields, depending on whether pressure dissipation is being applied or not. In Figure 3 we see the predictions of the pressure field for the FOAV scheme. Figure 3(a) shows the prediction where no dissipation is applied and Figure 3(b) shows where it is. In this case, we

notice that if no pressure dissipation is applied, then pressure wiggles occur near the corner of the step, which are smoothed out when dissipation is applied. For the SOAV scheme a similar pattern is observed, however, in this case the pressure wiggles have a slightly increased range downstream of 0.2 step heights from the corner of the step when no pressure dissipation is applied. Even so, when the pressure dissipation term is applied the pressure field is completely smooth. Predicting a smooth pressure field in the region around the step corner poses the greatest difficulties. Other authors have published 'non-staggered methodologies', which predict wiggles in this region, proving their methodology is not working, as it should [44]. In the present study, the predictions that use a pressure dissipation have completely smoothed out these strong wiggles without removing other pressure peaks, demonstrating a successful scheme. It is interesting to note, however, that there are no significant wiggles elsewhere in the solution away from the step corner and the inlet channel. Therefore, we could probably improve the current methodology by applying dissipation only in regions of the flow where it is needed; however, identifying where the dissipation is needed and how much should be applied is beyond the scope of this paper.

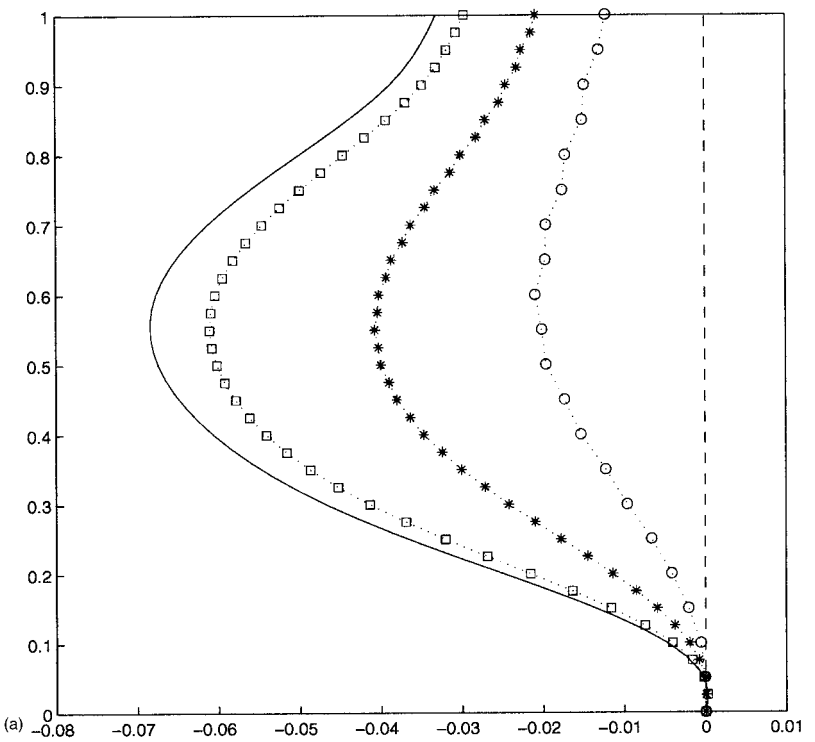

Figure 8. Pressure variation along the centreline of the cavity for $Re = 1000$ using the FOAV scheme, using 20×20 grid ○, 40×40 grid ∗, 60×60 grid □ and a 100×100 grid (—) for (a) no pressure dissipation and (b) applied pressure dissipation.

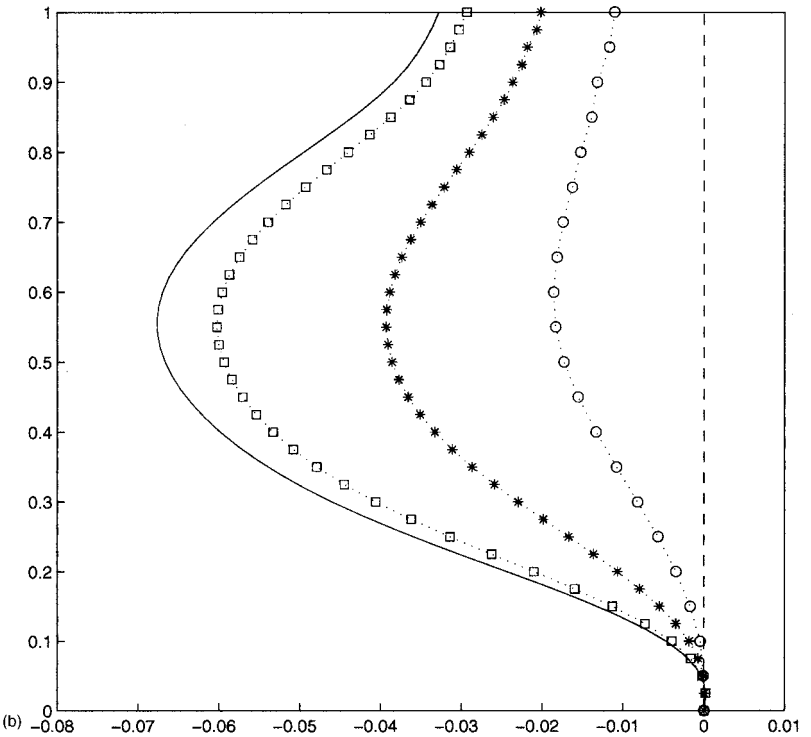

Figure 8 (*Continued*)

3.2. Laminar flow in a square cavity with a driven lid

A typical test for non-staggered methodologies is laminar flow in a square cavity with a driven lid using uniform grid distributions. The problem is illustrated in Figure 4. The illustration shows a large vortex in the middle of a square cavity that is created by a 'driven lid'. The symmetry and uniform distribution of the grid is suppose to amplify any problems that may be associated with the non-staggered methodology. For example, this problem and the similar problem of buoyancy-driven recirculation in a square cavity has been studied in a number of papers which test a non-staggered methodology, refer to, for example, References [25,26,32,45,46]. In this investigation various grid systems are employed consisting of 20×20, 40×40, 60×60 and 100×100 grid points.

In order to predict problems it is important to consider a high Reynolds number case; initially, results for $Re = 100$ were predicted, which is the same case study undertaken by Date [26]. However, it was not found to be a particularly interesting case because virtually no pressure oscillations were observed even for the 20×20 grid. We found that the predictions for the velocity profiles and pressure variation along the centre of the cavity did not require pressure dissipation for either differencing scheme. The SOAV scheme produced very similar

results for all four grids, maximum reverse flow of $-0.2U_{\mathrm{Lid}}$ and pressure peak of $-0.95\rho U_{\mathrm{Lid}}^2$. The results for the FOAV scheme slowly converged to the values for the 100×100 grid. These results demonstrate that the SOAV scheme is outperforming the FOAV scheme, it implies that pressure oscillations are strongly dependent on the local grid Reynolds number (grid Peclet number), but most importantly that the Reynolds number case is too low to be of any interest. So, we considered a much higher Reynolds number case, one of $Re = 1000$.

The Reynolds number is higher than typical values found in literature for the study of pressure wiggle suppression, however, there are available a variety of solutions for comparison [46,47]. In this case high pressure gradients are predicted, therefore, we feel the scheme is being tested well beyond normal limits. In Figure 5 results for the velocity profile are shown using the SOAV scheme. Figure 5(a) shows the velocity profile at the centre of the cavity, obtained from the various grids for the predictions that do not apply pressure dissipation and Figure 5(b) shows results from the various grids that do apply pressure dissipation. There is a single main recirculation region in the cavity, and we observe in the figure that the negative reverse flow has maximum of about 0.4 of the lid speed. This is slightly larger if no pressure dissipation is applied suggesting the application of pressure dissipation has a slightly deteriorating effect on the prediction of the velocity field. The velocity profiles from the various grids appear to change less dramatically for the solutions that do not apply pressure dissipation. This suggests that the addition of pressure dissipation is having an increasingly stronger effect for the coarser grids. This is a welcome outcome as pressure wiggles are dependent on the local grid Reynolds number. In comparison with the benchmark solutions of Ghia *et al.* [47], the results using the 60×60 and 100×100 grids are virtually identical. The SOAV scheme gives similar results for the finest grids used. The main difference is incurred with the use of the coarsest grid, though there is rapid improvement in the predictions with grid refinement. In Figure 6 we show the same set of results for the FOAV scheme. In terms of comparing the results that do and do not apply the pressure dissipation the exact same trends are observed; however, there is now the added complexity that the FOAV scheme fails to predict the results very accurately for any grid systems. Nonetheless, the important point is that the pressure wiggles (as implied with the previous set of results for $Re = 100$), do not appear to be strongly dependent on the type of differencing scheme used but dependent on the local grid Reynolds number.

In Figure 7, we initially consider predictions using the SOAV scheme. Figure 7(a) shows the variation of pressure along the centre of the cavity using various grids for the results that do not apply the pressure dissipation term, and Figure 7(b) shows the results that do apply the pressure dissipation term. Unlike the low Reynolds number results using the coarse grid we now observe significant differences depending on whether pressure dissipation is applied or not. The first difference is that the application of the pressure dissipation smoothes the pressure variation results successfully; this is a welcome result. However, the second difference is that the application of the pressure dissipation slightly deteriorates the overall results in comparison with the fine grid results. This is confirmed when analysing the overall pressure fields predicted. These results confirm that, by adding pressure dissipation, there is a slight deterioration in the overall accuracy of the results, which decreases with grid refinement, but (perhaps more importantly) that the pressure dissipation term successfully suppresses 'non-physical' wiggles in the pressure field.

In Figure 8, we show the predictions of pressure along the centre of the cavity for the FOAV scheme. In this case, there is a dramatic difference between the pressure variations using the various grids, unlike the previous set of results we observe that the results have not achieved grid-independency. This is because the FOAV scheme is being pushed well beyond its limits. The results from the fine and medium grids are comparable with their counterparts that do and do not apply pressure dissipation. This observation is just a demonstration that pressure wiggles are dependent on grid refinement and perhaps in the future with superior computing power, the need to apply pressure dissipation (and artificial viscosity) will become obsolete.

4. CONCLUDING REMARKS

The investigation demonstrated problems associated with non-staggered methodologies that have been previously observed. Namely, pressure wiggles are strongly dependent on flow conditions and grid refinement.

We have shown that odd–even coupling between the pressure and velocity fields can be suppressed by adding an additional fourth-order pressure dissipation term into the governing pressure equations. Using a semi-discretized approach to derive the governing algebraic equations allows us to derive equations that have a compact Laplacian for the governing pressure equation.

The non-staggered methodology was successfully tested on two standard laminar flow problems. In both test problems even for crude grid distributions and high cell Reynolds numbers no non-physical pressure wiggles are predicted provided a pressure dissipation is applied. Excessive application of the pressure dissipation will clearly lead to deterioration in the overall results. Therefore, limiting the amount of dissipation applied is probably a useful target for future work.

ACKNOWLEDGMENTS

The majority of this work was undertaken due to the encouragement and help of Professor J.E. Ffowcs Williams.

REFERENCES

1. Harlow FH, Welch JE. Numerical calculations of time-dependent viscous incompressible flow of fluid with free surface. *Physics in Fluids* 1965; **8**: 2182–2189.
2. Patankar SV, Spalding DB. A calculation procedure for heat, mass and momentum transfer in three-dimensional parabolic flows. *International Journal for Heat and Mass Transfer* 1972; **15**: 1787–1806.
3. Issa RI. Solution of the implicitly discretized fluid flow equations by operator-splitting. *Journal of Computational Physics* 1985; **62**: 40–65.
4. Pentaris A, Nikolados K, Tsangaris S. Development of projection and artificial compressibility methodologies using the approximate factorisation technique. *International Journal for Numerical Methods in Fluids* 1994; **19**: 1013–1038.
5. Patankar SV. *Numerical Heat Transfer and Fluid Flow*. Hemisphere: Washington, DC, 1980.
6. Peric M. A finite volume method for the prediction of three-dimensional fluid flow in complex ducts. PhD thesis, Mechanical Engineering Department, Imperial College, London, 1985.

7. Cheng L, Armfield S. A simplified marker and cell method for unsteady flows on non-staggered grids. *International Journal for Numerical Methods in Fluids* 1995; **21**: 15–34.
8. Rhie CM, Chow WL. Numerical study of the turbulent flow past an airfoil with trailing edge separation. *AIAA Journal* 1983; **21**: 1525–1532.
9. Miller TF, Schmidt FW. Use of a pressure-weighted interpolation method for the solution of incompressible Navier–Stokes equations on a nonstaggered grid system. *Numerical Heat Transfer* 1988; **14**: 213–233.
10. Han T. Computational analysis of three-dimensional turbulent flow around a bluff body in ground proximity. *AIAA Journal* 1989; **27**: 1213–1219.
11. Coelho PJ, Pereira JCF. Finite volume computation of the turbulent-flow over a hill employing 2D or 3D non-orthogonal collocated grid systems. *International Journal for Numerical Methods in Fluids* 1992; **14**: 423–441.
12. Melaaen MC. Analysis of fluid-flow in constricted tubes and ducts using body-fitted nonstaggered grids. *International Journal for Numerical Methods in Fluids* 1992; **15**: 895–923.
13. Kobayashi MH, Pereira JCF, Sousa JMM. Comparison of several open boundary numerical treatments for laminar recirculating flows. *International Journal for Numerical Methods in Fluids* 1993; **16**: 403–419.
14. Lai CJ, Yen CW. Turbulent free-surface flow simulation using a multilayer model. *International Journal for Numerical Methods in Fluids* 1993; **16**: 1007–1025.
15. Yeo RW, Wood PE, Hrymak AN. A numerical study of laminar 90-degree bend duct flow with different discretization schemes. *Transactions of the ASME, Journal of Fluids Engineering* 1991; **113**: 563–568.
16. Tsui YY, Lee SY. Calculation of turbulent flow through engine inlet ports. *International Journal for Heat and Fluid Flow* 1992; **13**: 232–240.
17. Davidson L. Prediction of the flow around an airfoil using a Reynolds stress transport model. *Transactions of the ASME, Journal of Fluids Engineering* 1995; **117**: 50–57.
18. Bohm M, Wechsler K, Schafer M. A parallel moving grid multigrid method for flow simulation in rotor stator configurations. *International Journal for Numerical Methods in Engineering* 1998; **42**: 175–189.
19. Gjesdal T, Lossius MEH. A general algorithm for compressible and incompressible flow. *International Journal for Numerical Methods in Fluids* 1997; **25**: 393–405.
20. Armfield SW. Finite difference solutions of the Navier–Stokes equations on staggered and non-staggered grids. *Computers in Fluids* 1991; **20**: 1–17.
21. Armfield SW. Fourth order elliptic correction for the Navier–Stokes equations on non-staggered grids. In *Computational Techniques and Applications*, May RL, Easton AK (eds). Springer-Verlag: London, 1996; 113–119.
22. Coates MJ, Patterson JC. Numerical simulations of the natural convection in a cavity with nonuniform internal sources. *International Journal for Heat and Fluid Flow* 1994; **15**: 218–225.
23. Reggio M, Camarero R. Numerical solution for viscous incompressible flows. *Numerical Heat Transfer* 1986; **10**: 131–146.
24. Thiart GD. Finite difference scheme for the numerical solution of fluid flow and heat transfer problems on non-staggered grids. *Numerical Heat Transfer B* 1990; **17**: 43–62.
25. Harms TM, von Backstrom TW, du Plessis JP. Reformulation of the SIMPLEN discretization scheme to accommodate noncentralized interfaces. *Numerical Heat Transfer B* 1991; **20**: 127–144.
26. Date AW. Solution of Navier–Stokes equations on non-staggered grids. *International Journal for Heat and Mass Transfer* 1993; **36**: 1913–1922.
27. Williams M. A Helmholtz pressure equation method for the calculation of unsteady incompressible viscous flows. *International Journal for Numerical Methods in Fluids* 1992; **14**: 1–12.
28. Shih TM, Ren AL. Primitive variable formulations using non-staggered grids. *Numerical Heat Transfer* 1984; **7**: 413–428.
29. Chorin AJ. Numerical solutions of the Navier–Stokes equations. *Mathematics in Computers* 1968; **22**: 745–762.
30. Patel MK, Markatos NC. An evaluation of eight discretization schemes for two-dimensional convection–diffusion equations. *International Journal for Numerical Methods in Fluids* 1986; **6**: 129–154.
31. Fletcher CAJ. *Computational Techniques for Fluid Dynamic*, vol. II. Springer: Berlin, 1988.
32. Lee SL, Tzong RY. Artificial pressure for pressure-linked equation. *International Journal for Heat and Mass Transfer* 1992; **35**: 2705–2716.
33. Hirsch C. *Numerical Computation of Internal and External Flows, Vol. 1: Fundamentals of Numerical Discretization*. Wiley: New York, 1989.
34. Majumdar S. Role of under-relaxation in momentum interpolation for calculation of flow with staggered grids. *Numerical Heat Transfer* 1988; **13**: 125–132.
35. Anderson DA, Tannehill JC, Pletcher RH. *Computational Fluid Mechanics and Heat Transfer*. Hemisphere: Washington, DC, 1984.
36. Barton IE. A numerical study of flow over a confined backward facing step. *International Journal for Numerical Methods in Fluids* 1995; **21**: 653–665.

37. Shyy W. A study of finite difference approximations to steady-state, convection-dominated flow problems. *Journal of Computational Physics* 1985; **57**: 415–438.
38. Armaly BF, Durst F, Pereira JCF, Schönung B. Experimental and theoretical investigation of backward-facing step flow. *Journal of Fluid Mechanics* 1983; **127**: 473–496.
39. Thangam S, Knight DD. Effect of stepheight on the separated flow past a backward facing step. *Physics of Fluids A* 1989; **1**: 604–606.
40. Gartling DK. A test problem for outflow boundary conditions—flow over a backward-facing step. *International Journal for Numerical Methods in Fluids* 1990; **11**: 953–967.
41. Lee D, Tsuei YM. A modified adaptive grid method for recirculating flows. *International Journal for Numerical Methods in Fluids* 1992; **14**: 775–791.
42. Barton IE. The computation of the entrance effect for laminar flow over a backward-facing step. *International Journal for Numerical Methods in Fluids* 1997; **25**: 633–644.
43. Sani RL, Gresho PM. Résumé and remarks on the open boundary condition minisymposium. *International Journal for Numerical Methods in Fluids* 1994; **18**: 983–1008.
44. Le TH, Troff B, Sagaut P, Dang-Tran K, Phuoc LT. Pegase: a Navier–Stokes solver for direct numerical simulation of incompressible flows. *International Journal for Numerical Methods in Fluids* 1997; **24**: 833–861.
45. Choi SK, Nam HY, Cho M. Systematic comparison of finite-volume calculation methods with staggered and nonstaggered grid arrangements. *Numerical Heat Transfer B* 1994; **25**: 205–221.
46. Choi SK, Nam HY, Cho M. A comparison of higher-order bounded convection schemes. *Computational Methods in Applied Mechanics Engineering* 1995; **121**: 281–301.
47. Ghia U, Ghia KN, Shin CT. High *Re* solutions for incompressible flow using the Navier–Stokes equations and a multigrid method. *Journla of Computational Physics* 1982; **48**: 387–411.

